

INFLUENCE OF THE SURFACE ENERGY OF A BASALT FIBER ON CAPILLARY WICKING AND IN-PLANE PERMEABILITY

R. Ravel¹, M.F. Pucci², P.J. Liotier³

¹ PCH, IMT Mines Alès, Univ Montpellier, Alès, France, romain.ravel@mines-ales.fr

² DMS, IMT Mines Alès, Univ Montpellier, LMGC UMR 5508, Alès, France,
monica.pucci@mines-ales.fr

³ PCH, IMT Mines Alès, Univ Montpellier, Alès, France, pierre-jacques.liotier@mines-ales.fr

Keywords: Wettability, Basalt fiber, Liquid composite moulding, Surface energy, Capillary wicking, In-plane permeability

ABSTRACT

The present work focuses on the influence of the surface energy modification of basalt fibers on the fiber wettability at different scales: a single fiber, a strip of fabric and a fibrous preform representative for Liquid Composite Moulding (LCM) processes. To modify the initial surface energy of the basalt fiber, a thermal treatment was used (4h at 400°C). The experimental approach used is as follows: firstly, the surface energy of the modified single fiber was determined, secondly the capillary wicking and the capillary pressure (P_{cap}) of the fabric were estimated and finally the in-plane unsaturated permeability of the fibrous preform was characterized. The results showed that, after thermal treatment, the surface energy of single basalt fibers is higher, particularly due to the increase of 18% of its polar component. The wicking kinetic was faster and the P_{cap} increased of 100% in spontaneous impregnation regime. The in-plane unsaturated permeability value of the fibrous preform also rose of 42% in forced regime. In conclusion, the thermal treatment performed improved the wettability between the basalt fiber and the water. Moreover, in the study conditions, the capillary effects proved to be non-negligible on the unsaturated permeability measurement.

1 INTRODUCTION

The understanding and the characterization of the wettability in fibrous reinforcements at different scales is a major challenge in the liquid composite moulding (LCM) processes [1]. Indeed, wettability properties of the fibrous preform depend on several parameters such as the flow regime and the surface properties of fibers and liquid. Furthermore, under specific conditions of flow, capillary effects are susceptible to have a non-negligible effect on the unsaturated permeability results [2]. The aim of this work is to highlight the influence of the surface energy modification of a basalt fiber on the improvement of the wettability with a defined liquid (water) at different scales (a single fiber, a strip of fabric and a fibrous preform). For this, the basalt fibers were thermally treated to modify their surface properties [3, 4]. For each scale, a specific experiment was performed: characterization of the surface energy of single fibers, characterization of the capillary wicking and the P_{cap} of fabrics and finally characterization of the unsaturated permeability of the fibrous preforms. The originality of this work is to connect the different scales by demonstrating experimentally that the surface energy of single fibers influences the spontaneous impregnation properties (capillary wicking and P_{cap}), and that this effect also propagates on the unsaturated permeability of the fibrous preform in forced impregnation. Results show that, under the tested process conditions and with the considered fibre-liquid couple, the capillary effects are not negligible in the in-plane unsaturated permeability measurement.

2 MATERIALS AND METHODS

2.1 Basalt fibers

The quasi-unidirectional basalt fabric chosen for this study was supplied by BASALTEX NV (Belgium, Wevelgem, reference BAS UD400). This fabric, with a nominal surface area of 430g/m², has

a heat-bonded glass yarn in the weft direction. Fibers present an epoxy compatible sizing (silane-based). In the study, these fibers are called “as received”.

2.2 Thermal treatment

The aim of this work is to evaluate the influence of the surface modification of basalt fibers on the impregnation of fabric and then on the LCM process. To do this, a thermal treatment was performed to remove the sizing and consequently modify the surface energy. The thermal treatment is based on previous works of our team [4], showing that a treatment of 4h at 400°C (under air) leads to a higher surface energy with a higher polar component. In the study, the thermal modified fibers are called “thermally treated”.

2.3 Morphological characterizations of the fibers

The fiber surface morphology before and after treatment was observed with a scanning electron microscope (SEM) supplied by FEI: QUANTA 200 FEG. The basalt fiber diameter was measured and the homogeneity and the repartition of the sizing were observed. The partial or complete un-sizing was then evaluated for “thermally treated” fibers.

2.4 Contact angle characterization: tensiometric method

The contact angles between single fibers and several liquids were characterized with a force tensiometer supplied by KRÜSS (Germany): K100SF. This force tensiometer is characterized by a high precision balance with a resolution of 10^{-7} g, which makes possible the weighing of a meniscus formed by a liquid around a single fiber. This method was well described by W. Garat et al. in a previous work [5]. For each liquid-fiber couple, an equilibrium contact angle is determined using the Wilhelmy relation (Equation 1):

$$F_c = ma = p\gamma_L \cos \theta \quad (1)$$

With F_c the capillarity force, m the meniscus weight, a the acceleration, p the wetting perimeter, γ_L the liquid surface tension and θ the contact angle.

Firstly, single fiber is bonded on plastic support called “tab” with a UV adhesive (Dymax Europe GmbH, reference: 3193). Secondly, the wetting perimeter of the single fiber is determined by making an experiment with a totally wetting liquid: the n-Hexane ($\theta = 0$). Finally, the contact angles (θ_c) with four liquids (n-Hexane, diiodomethane, ethylene glycol and water (Table 1)) are determined making tests on the same fiber, as detailed in [5]. This work was performed on “as received” and “thermally treated” fibers. To check the reproducibility, 5 fibers of both references were tested.

Test liquids	η (mPa.s)	ρ (g/cm ³)	γ_L^P (mN/m)	γ_L^d (mN/m)	γ_L (mN/m)
n-Hexane	0.32	0.659	0.0	18.4	18.4
Diiodomethane	2.76	3.325	2.3	48.5	50.8
Ethylene glycol	21.81	1.113	19	29	48
Water	1.00	0.998	51.0	21.8	72.8

Table 1: Test liquids properties.

2.5 Surface energy determination

Once the contact angle of the basalt fiber with each liquid is known, the surface energy was calculated by using the Owens and Wendt equation (Equation 2) combined with the Young-Laplace equation (Equation 3). The combination of both equations (2 and 3) gives the equation 4.

$$\gamma_S + \gamma_L - \gamma_{SL} = 2\sqrt{\gamma_S^d \gamma_L^d} + 2\sqrt{\gamma_S^P \gamma_L^P}, \quad (2)$$

$$\cos \theta_e = \frac{\gamma_S - \gamma_{SL}}{\gamma_L}, \quad (3)$$

$$\gamma_L(1 + \cos \theta_e) = 2\sqrt{\gamma_S^d \gamma_L^d} + 2\sqrt{\gamma_S^P \gamma_L^P}. \quad (4)$$

With the Equation 4, the two components (polar and dispersive) of the surface energy can be determined by knowing the contact angle with at least two liquids. In this work, to increase the accuracy, four liquids were used and the linearized form of the Owens and Wendt equation was used, as follows:

$$\underbrace{\frac{\gamma_L(1 + \cos \theta_e)}{2\sqrt{\gamma_L^d}}}_Y = \underbrace{\sqrt{\gamma_S^P} \left(\frac{\sqrt{\gamma_L^P}}{\sqrt{\gamma_L^d}} \right)}_X + \sqrt{\gamma_S^d}. \quad (5)$$

By drawing the curve of the parameter Y as a function of X for each liquid with the θ_e determined experimentally and the liquid surface tension (Table 1), the polar and dispersive components of fiber surface energy can be determined from the linear regression equation (Equation 4). This method was applied for both fibers “as received” and “thermally treated”.

2.6 Capillary pressure determination: wicking tests

The method used here was developed in a previous work [6]. A roll of fabric was inserted in a cylindrical simple holder with an inner diameter of 12mm and a height of 20mm. The fabric length was calculated to obtain a fiber volume fraction of 40%. The capillary wicking tests were performed in the longitudinal direction of the fabric. These experiments were performed with a DCAT11 force tensiometer supplied by Dataphysics Instrument GmbH (Fildestrardt, Germany). The resolution of the high precision balance is 10^{-5} g. Firstly, the sample holder containing the fabric is fixed to the tensiometer. Then, the vessel containing the solvent is placed under the sample holder. The vessel rises at a speed of 0.5mm/s until to get in touch with the fabric. After the contact, the vessel stays in its position and the mass gain (m) over time (t) is recorded.

In a first step, the experiment is realized with n-Hexane to determine the morphology parameters of the porous media, specifically the $c\bar{r}$ (c is a parameter relating to the tortuosity of the media and \bar{r} is representative of the mean capillary radius), present in the modified Washburn equation for a porous medium in a tube (Equation 6).

$$m^2(t) = \left[\frac{(c\bar{r})\varepsilon^2(\pi R^2)}{2} \right] \frac{\rho^2 \gamma_L \cos \theta_a}{\eta} t. \quad (6)$$

With ε the relative porosity, R the inner radius of the cylindrical simple holder and ρ the density, η the viscosity, and γ_L the surface tension of the test liquid. Once the morphology parameter determined with n-Hexane, the advancing contact angle θ_a with water can be determined by the fit of the recorded curve (m^2 vs t) with the Washburn equation (Equation 6). To verify the reproducibility of tests, five samples of each reference (“as received” and “thermally treated”) were performed with n-Hexane and water.

The method used to calculate the equivalent capillary pressure has already been well described in previous work by M.F. Pucci et al. [6]. This definition of P_{cap} (Equation 7) was based on an equivalence between the Washburn equation and the Darcy law, which considers:

- $c\bar{r}$: the morphology of the porous medium as defined above,
- ε : the porosity of the porous medium,
- K: the saturated permeability of the porous medium,
- γ_L and θ_a : the surface tension of the test liquid and the advancing contact angle representing the fluid/porous medium interactions.

$$P_{cap} = (c\bar{r})\varepsilon \frac{\gamma_L \cos(\theta_a)}{4K}. \quad (7)$$

2.6 In-plane permeability tests

To characterize the impact of the surface modification of fibers at the process scale, in-plane unsaturated permeability tests were performed. The device is a prototype developed and made in IMT Mines Alès. This prototype is composed of an aluminium bottom mould of 20mm of thickness and a transparent PMMA top mould of 100mm of thickness. Between both parts, an aluminium frame of 3mm of thickness is placed to receive the fibrous preform. The internal dimensions of the frame are: 400x150mm. The bottom mould is composed of two holes at the two extremities of the preform to ensure the inlet and the outlet of the fluid. An area of 1cm of width is left empty in the inlet side to allow a good fluid distribution along the entire width of the preform (Fig. 1).

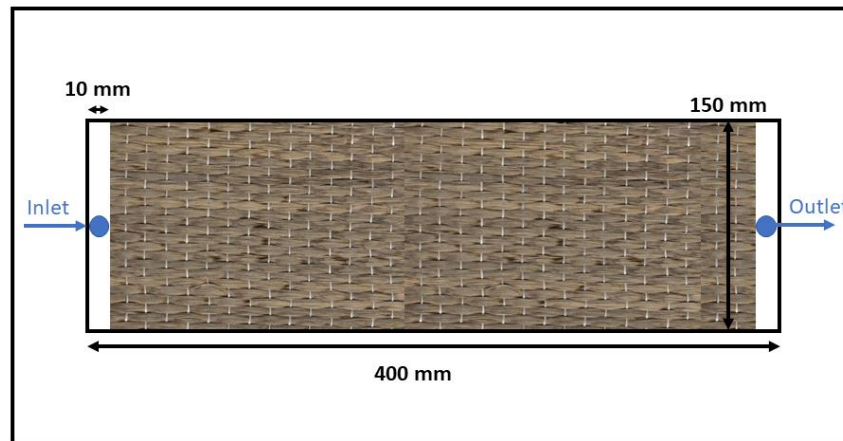


Figure 1: Schematic representation of the permeability prototype size.

To ensure the sealing between the three parts of the prototype (bottom, top and frame), o-rings and sealing grease were used all around of the preform area. The mould is closed with sixteen screws tightened with a torque of 25Nm. Fluid is injected with a pressure between 0.61bar and 0.67bar with a single component injection tank supplied by ISOJET Equipements (Corbas, France). The inlet and the outlet of the bottom mould are equipped with two pressure sensors (Keller, PR35X serie).

To determine the in-plane unsaturated permeability [7, 8], the flow front acquisition was recorded with a color camera supplied by SVS-Vistek (reference: EXO252CU3), and a fixed lens (12mm / F2.8) supplied by Computar (reference M1228-MPW3). The image processing was automatically performed with a program developed by LabVIEW.

The fiber volume fraction for the test was fixed at 53.7%, which represents 10 plies in a frame of 3mm of thickness. The liquid used for these experiments was water. To verify the reproducibility, two experiments with water were performed for each reference (“as received” et “thermally treated”).

3 RESULTS AND DISCUSSIONS

3.1 Basalt fiber morphology

Basalt fibers were observed by SEM to characterize the morphology and the diameter before and after thermal treatment. As shown in figure 2(a), fibers “as received” had some small deposits distributed heterogeneously on the surface.

Figure 2(b) presents the “thermally treated” fibers: their surfaces appeared perfectly smooth and homogeneous. Visually, the thermal treatment seems to remove the entirety of the sizing.

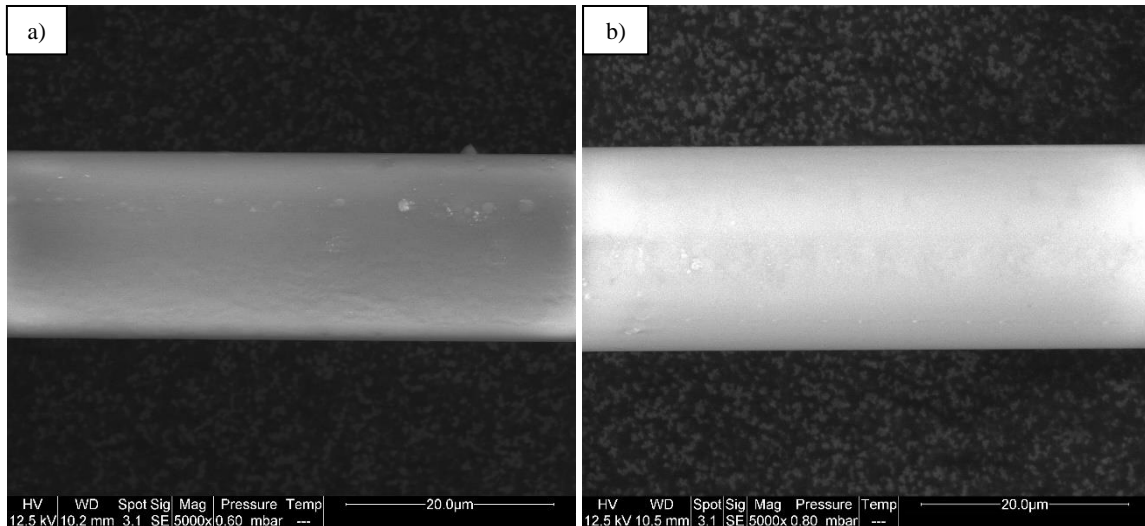


Figure 2: SEM images of (a) “as received” and (b) “thermally treated” basalt fibers.

The impact of the thermal treatment on the diameter value was observed by SEM images and tensiometric measurement. The table 2 summarizes the diameters measured before and after treatment and shows that the thermal treatment did not significantly modify the fiber diameters.

	“As received” fibers	“Thermally treated” fibers
Average diameter (μm)	18.3	18.9
Standard deviation (μm)	0.5	0.6

Table 2: Average diameter before and after thermal treatment – SEM images.

	“As received” fibers	“Thermally treated” fibers
Average diameter (μm)	18.3	18.5
Standard deviation (μm)	0.8	1.9

Table 3: Average diameter before and after thermal treatment – tensiometric method.

Table 3 presents the results of diameter measurements by tensiometric method. Results obtained with both methods before and after thermal treatment are very similar. The un-sizing step doesn’t seem to have a significant impact on the fiber diameter. The next step of the study is to evaluate the impact of this surface modification on the surface energy value, and especially on polar and dispersive components.

3.2 Contact angle determination at the single fiber scale

Tables 4 presents the contact angles of the “as received” and “thermally treated” fibers with the four solvents chosen for the study (n-Hexane, diiodomethane, ethylene glycol and water). Contact angles before and after treatment are similar for the diiodomethane and the ethylene glycol. In contrast, for water, the average contact angle obtained after thermal treatment is significantly lower: 34.5° instead of 44.6°. This decrease of angle should indicate a better wettability of the “thermally treated” fiber by the water.

Average Values	$\theta_{\text{n-Hexane}} (^{\circ})$	$\theta_{\text{water}} (^{\circ})$	$\theta_{\text{diiodo}} (^{\circ})$	$\theta_{\text{ethylene glycol}} (^{\circ})$
"As received" basalt fiber	0	44.6 ± 3.4	51.0 ± 4.0	46.7 ± 2.7
"Thermally treated" basalt fiber	0	34.5 ± 4.1	48.0 ± 2.0	47.9 ± 2.0

Table 4: Static contact angles – “As received” and “Thermally treated” basalt fibers.

3.3 Fiber surface energy determination

Figures 3 and 4 represent respectively the application of the Owens and Wendt method described in section 2.5 for the “as received” and “thermally treated” basalt fibers.

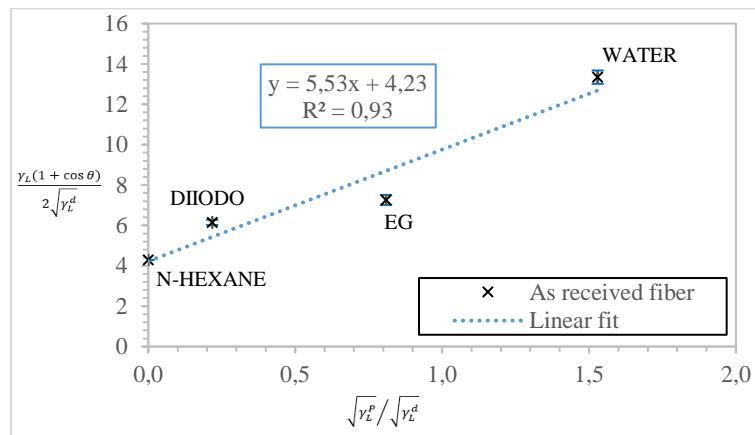


Figure 3: Surface energy – “as received” basalt fiber.

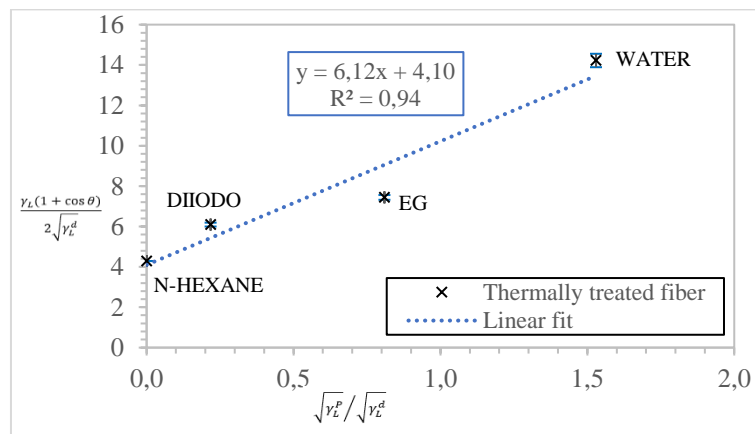


Figure 4: Surface energy – “thermally treated” basalt fiber.

For both, the linear fit of the Owens and Wendt method was well applied: the correlation coefficients were found to be greater or equal to 0,93. Table 5 presents the surface energy results.

Basalt fiber	γ_s^P (mN/m)	γ_s^d (mN/m)	γ_s (mN/m)
As received	30.6 ±2.1	17.9 ±0.4	48.5 ±2.5
Thermally treated	37.5 ±2.3	16.8 ±0.1	54.3 ±2.4

Table 5: Dispersive (γ_s^d), polar (γ_s^P) and total (γ_s) surface energy of the “as received” and “thermally treated” basalt fibers.

Standard deviations are low, between 2mN/m and 2.5mN/m, demonstrating the accuracy and the repeatability of the results. Table 5 shows that the dispersive component γ_s^d before and after thermal treatment did not change. However, the polar component γ_s^P increases by approximately 18% after thermal treatment. Consequently, the total surface energy also increases. Results confirm that the thermal un-sizing leads to increase the surface energy of the basalt fiber and especially the polar component.

3.4 Equivalent capillary pressure estimation

Table 6 presents $c\bar{r}$ (obtained with n-Hexane) et θ_a (with water) results for the quasi-unidirectional basalt fabric before and after thermal treatment. Experiments were performed on five samples for both references. Figures 5 shows the capillary wicking curves with water of the “as received” and the “thermally treated” fabrics. It is observed that the wicking kinetic is significantly faster after treatment.

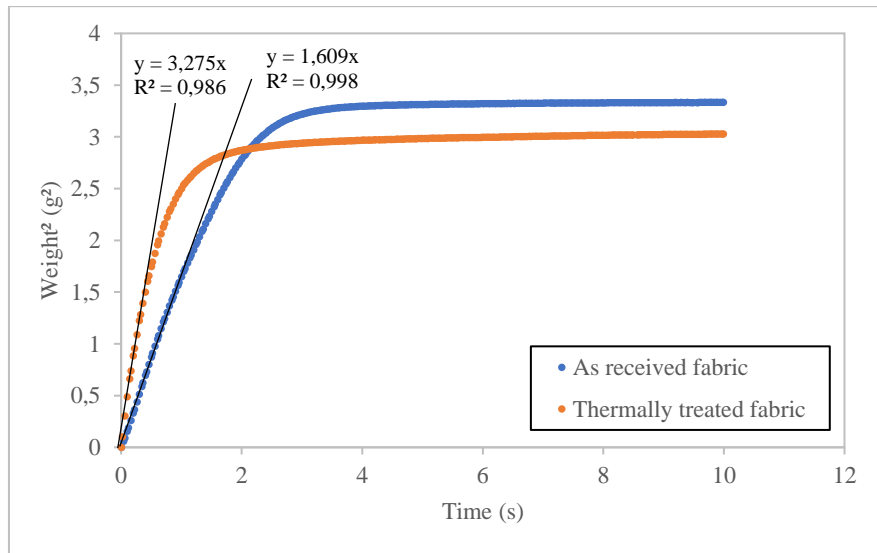


Figure 5: Capillary wicking test with water

Basalt fiber	$c\bar{r}$ (μm)	θ_a water ($^\circ$)
As received	33.62 ±2.86	72.6 ±0.9
Thermally treated	22.47 ±7.06	27.3 ±8.6

Table 6: $c\bar{r}$ et θ_a (water) results – Quasi UD basalt fiber – before and after thermal treatment.

Table 6 shows that the $c\bar{r}$ factor decreased after thermal treatment. The SEM observations didn't show a surface modification of fiber after treatment, this morphological factor should not vary a lot. However, removal of the sizing affected the arrangement of the fibers between them. After thermal

treatment, fibers are more mobile in relation to each other and then, during their positioning in the cylindrical sample holder, they may have been able to reorganise themselves differently compared to the “as received” fibers. In Table 6, it is observed that the average advancing contact angle with water decreased significantly after treatment. This reduction of contact angle (27.3° after treatment again 72.6° before) seems to be coherent with the results at the scale of single fiber.

After having determined experimentally the geometrical factor ($c\bar{r}$) and the Washburn contact angle with water (θ_a), it becomes possible to calculate an equivalent capillary pressure (Equation 7). In this equation, the saturated permeability value needs to be determined. This parameter was determined using the Gebart equation and considering a hexagonal arrangement [9]. Table 7 presents the equivalent capillary pressure calculated for both references.

Basalt fiber	P_{cap} (KPa)
As received	6.6 ± 0.3
Thermally treated	13.2 ± 1.2

Table 7: Equivalent capillary pressure with water – before and after thermal treatment.

After thermal treatment, the advancing contact angle significantly decreased and the capillary pressure doubled in value (Table 7). These two observations lead to say that surface modification by thermal treatment significantly affects the spontaneous impregnation.

3.5 In-plane unsaturated permeability estimation

Finally, the last step of this work is to highlight the impact of the surface modification at the scale of the process with a stack of 10 plies of the quasi-unidirectional basalt fabric.

Figure 6 shows the standard curve of the squared front fluid position as a function of time obtained with the acquisition of the average advancement of the fluid front.

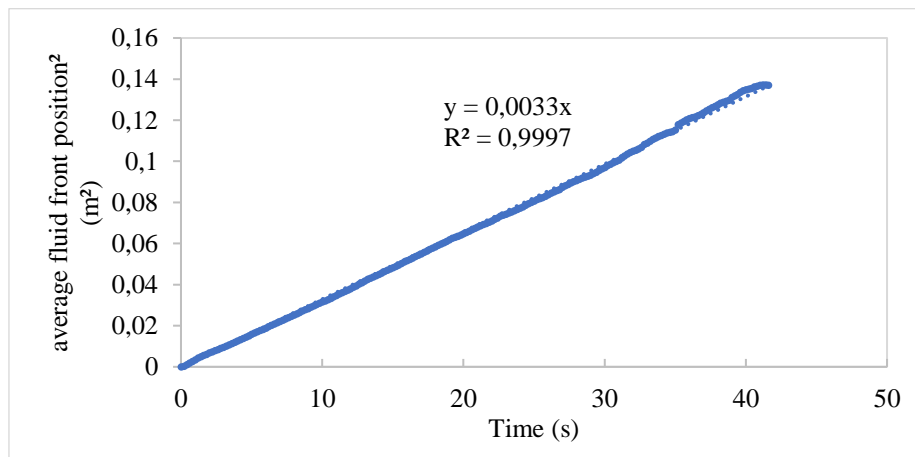


Figure 6: squared flow front position vs time – “as received” basalt fabric/water.

The method used to calculate the unsaturated permeability is based on the Squared Flow Front method described in the second permeability Benchmark of N. Vernet et al. (Equation 8) [7].

A linear fit can be plotted from the curve squared front fluid position vs time (Equation 9), then with the slope m of the linear trend (Equation 10), the unsaturated permeability can be calculated according to the Darcy’s Law (Equation 11).

$$K_{unsat} = \frac{x_{ff}^2 \varepsilon \mu}{2P_{inj} t}, \quad (8)$$

$$x_{ff}^2 = \frac{K_{unsat} 2P_{inj}}{\varepsilon \mu} t, \quad (9)$$

$$m = \frac{K_{unsat} 2P_{inj}}{\varepsilon \mu}, \quad (10)$$

$$K_{unsat} = \frac{m \varepsilon \mu}{2P_{inj}}. \quad (11)$$

With m the slope of the linear trend, ε the relative porosity, μ the fluid viscosity and P_{inj} the injection pressure of the fluid.

Table 8 presents the results of unsaturated permeability experiments with water for both references.

Basalt fiber	$K_{unsaturated}$ (m ²)
10 plies quasi-UD “as received”	$1.106 \times 10^{-11} \pm 0.044 \times 10^{-11}$
10 plies quasi-UD “thermally treated”	$1.581 \times 10^{-11} \pm 0.089 \times 10^{-11}$

Table 8: Unsaturated permeability results of quasi-UD “as received” and “thermally treated”.

After thermal treatment, the unsaturated permeability value increase by 1.106×10^{-11} to 1.581×10^{-11} m² with a low standard deviation (0.089×10^{-11} m² to the maximum), this increase means that the preform is more permeable and so the flow speed in the preform is quicker. Once again, these results at the scale of process seems coherent to ones at the scale of fabric and at the scale of fiber. The wettability of the basalt fabric preform with water is well improved at the process scale after the thermal treatment.

4 CONCLUSIONS

In the present work, the influence of the surface modification of basalt fibers on the spontaneous impregnation of a fabric and the unsaturated permeability has been evaluated.

It can be concluded that the thermal treatment performed affects:

- the surface energy of the single basalt fibers by increasing particularly its polar component by 18%,
- the capillary wicking by rising significantly the P_{cap} from 6.6KPa to 13.2KPa in spontaneous impregnation regime with water,
- the in-plane unsaturated permeability by rising its value from 1.11×10^{-11} m² to 1.58×10^{-11} m² for the fibrous preform with water.

Therefore, the experimental approach used enabled to observe that the capillary effects are not negligible compared to the viscous forces in unsaturated permeability tests under specific conditions (process and optimal fibre-resin compatibility parameters).

ACKNOWLEDGEMENTS

The authors thank the mechanical platforms of IMT Mines Alès and the Engineering school of Mines de Saint-Etienne for their help with the manufacturing of the permeability prototype, Prof. Slangen and Mr. Lorquet for their advice for the choice of the camera and settings and Mr. Chéron for his help in the development of the LabView program for the permeability measurements.

REFERENCES

- [1] J-H. Kim, D-J. Kwon, L.K. DeVries, J-M Park, Innovative wicking and interfacial evaluation of carbon fiber (CF)/Epoxy composites by CF tow capillary glass tube method (TCGTM) with Tripe-CF fragmentation test, *Composites Science and Technology*, **25**, 2022, 109495 (<https://doi.org/10.1016/j.compscitech.2022.109495>).
- [2] J. Verrey, V. Michaud, J.-A.E. Manson, Dynamic capillary effects in liquid composite moulding with non-crimp fabrics, *Composites Part A*, **37**, 2006, pp. 92–102 (<https://doi.org/10.1016/j.compositesa.2005.04.011>).
- [3] H. Liu et al., A Review on Basalt Fiber Composites and Their Applications in Clean Energy Sector and Power Grids, *Polymers* 2022, **14**, 2022, 2376 (<https://doi.org/10.3390/polym14122376>).
- [4] M. F. Pucci et al., Surface characterisation and wetting properties of single basalt fibres, *Composites Part B*, **109**, 2017, pp 72-81 (<https://doi.org/10.1016/j.compositesb.2016.09.065>).
- [5] W. Garat et al., Surface energy determination of fibres for Liquid Composite Moulding processes: Method to estimate equilibrium contact angles from static and quasi-static data, *Colloids and Surfaces A*, **611**, 2021, 125787, (<https://doi.org/10.1016/j.colsurfa.2020.125787>).
- [6] M. F. Pucci, P-J Liotier, S. Drapier, Capillary wicking in a fibrous reinforcement – Orthotropic issues to determine the capillary pressure components, *Composites Part A*, **77**, 2015, pp. 133-141 (<https://doi.org/10.1016/j.compositesa.2015.05.031>).
- [7] N. Vernet et al., Experimental determination of the permeability of engineering textiles: Benchmark II, *Composites Part A*, **61**, 2014, pp. 172-184 (<https://doi.org/10.1016/j.compositesa.2014.02.010>).
- [8] G. Francucci, E. S. Rodríguez, A. Vázquez, Study of saturated and unsaturated permeability in natural fiber fabrics, *Composites Part A*, **41**, 2010, pp. 16-21 (<https://doi.org/10.1016/j.compositesa.2009.07.012>).
- [9] B. R. Gebart, Permeability of Unidirectional Reinforcement for RTM, *Journal of Composite Materials*, **26**, 1992, pp. 1100-1133 (<https://doi.org/10.1177/002199839202600802>).